FISEVIER

Contents lists available at ScienceDirect

## Materials and Design

journal homepage: www.elsevier.com/locate/matdes



# 3D cellular metamaterials with planar anti-chiral topology



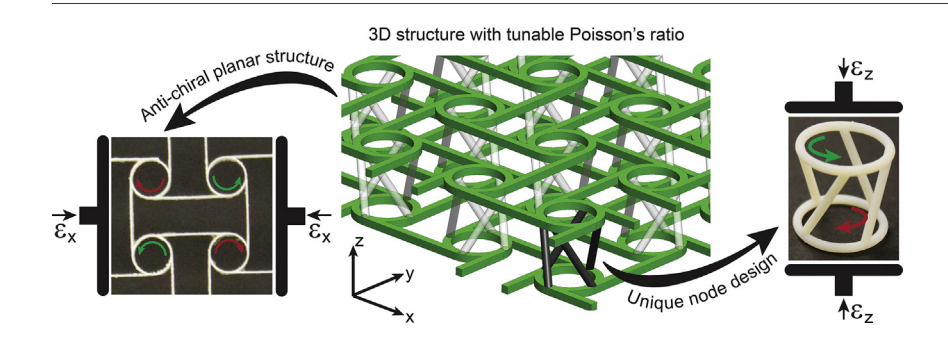
Hamid Ebrahimi <sup>a</sup>, Davood Mousanezhad <sup>a</sup>, Hamid Nayeb-Hashemi <sup>a</sup>, Julian Norato <sup>b</sup>, Ashkan Vaziri <sup>a,\*</sup>

- <sup>a</sup> Department of Mechanical and Industrial Engineering, Northeastern University, Boston, MA 02115, USA
- <sup>b</sup> Department of Mechanical Engineering, University of Connecticut, Storrs, CT 06269, USA

#### HIGHLIGHTS

- A new class of 3D cellular metamaterials introduced with tunable Poisson's ratio.
- Wide range of Poisson's ratios, both positive and negative values, is achievable.
- The behavior of the structure is governed by three geometrical parameters.
- The design concept provides a framework to develop auxetic cellular materials.

#### GRAPHICAL ABSTRACT



### ARTICLE INFO

Article history: Received 20 November 2017 Received in revised form 6 February 2018 Accepted 17 February 2018 Available online 19 February 2018

Keywords: Cellular material Auxetic behavior Poisson's ratio Chirality

### ABSTRACT

We constructed a new class of three-dimensional cellular metamaterials by connecting planar structure with anti-chiral topology. This was achieved by introducing a unique node design for connecting planar materials to enable constructing a three-dimensional architecture. This node design is based on linking the circular elements of the anti-chiral topology using oblique load-bearing ligaments. As the planar structure is subjected to loading, the circular elements rotate and the ligaments undergo bending, resulting in out-of-plane deformation of the three-dimensional cellular metamaterials. The node design, and specifically the ligaments' revolution angle govern the behavior of cellular metamaterials. This was demonstrated by designing cellular metamaterials with a wide range of positive and negative Poisson's ratio in the out-of-plane direction.

© 2018 Elsevier Ltd. All rights reserved.

Chirality, a common topological feature in natural systems [1–5], has been recently used in development of metamaterials with unusual properties such as negative refractive index [6–9] and aircraft morphing structures [10,11]. Some chiral structures are shown to have negative Poisson's ratio, also known as auxeticity [12,13], which is an unconventional property also observed in other architectured materials such as re-entrant, rotating-units, and hierarchical structures as well as in multistable architected materials and materials with instability-induced auxeticity [14–23]. Auxeticity can indirectly alter other mechanical properties of such structures through increased fracture toughness,

shear stiffness and indentation resistance [16,24–27], while also enabling the structure to undergo dramatic shape changes and large strains [28–30]. These characteristics highlights the potential application of auxetic metamaterials in developing novel fasteners [31], bioprostheses [32], expandable stents [33–35], dome shaped panels [36,37], multifunctional nanolattices [38], and foams with high structural integrity [39].

Reflecting the potential application of auxeticity there has been a surging interest in developing 3D auxetic structures [40–44]. For example, Li et al. [45] introduced a novel 3D augmented cellular structure based on re-entrant units that exhibits high Young's modulus and negative Poisson's ratio. Buckling induced auxeticity [17,46,47] and cross-chirality [43,48] are among other strategies used in development of

<sup>\*</sup> Corresponding author.

E-mail address: vaziri@coe.neu.edu (A. Vaziri).

three dimensional cellular structures with novel multifunctional properties. Ha et al. [49] developed a chiral three-dimensional cubic lattice with Poisson's ratio tunable over a narrow range that included negative values. Buckmann et al. [50] used dip-in direct-laser-writing to fabricate a three-dimensional complex microstructure with Poisson's ratio in the range of -0.12 and 0.13. The same group also introduced another design [51] for 3D structures that can exhibit Poisson's ratio as low as -1.

In this paper, we introduce a new 3D lattice structure that is based on connecting planar anti-chiral cellular materials using a unique node design, enabling the extension of the material in the out-ofplane direction. Unlike previously studied 3D structures [17,40-42,46,47] that only achieve negative or positive Poisson's ratio, and also generally have a narrow range of possible Poisson's ratio values, our proposed 3D cellular metamaterial can achieve a wide range of Poisson's ratio –from positive values to negative values– by changing the node geometrical parameters. This simple yet effective design is presented in Fig. 1. Part (a) shows a 3D printed sample of an anti-tetra-chiral structure, which forms the planar base for our final architecture. This planar structure is constructed by circular elements that are connected to each other with straight ligaments. The ability of these ligaments to "wind" around circular elements gives them the unusual property of negative Poisson's ratio [12,52]. More specifically the ratio of diameter of circular element to length of ligaments, D/a, controls the value of Poisson's ratio at large deformation. A schematic of the unit cell of this planar structure is shown in Fig. 1b with arrows showing the direction of rotation of circular element under compressive loading. We harness the rotation pattern induced by in-plane deformation and combine it with a unique 3D node design to control deformation in out of plane direction. The 3D node shown in Fig. 1b (right) consists of inclined ligaments that connect the top and bottom circular elements resembling the form of a cylinder. Assuming the ligaments to be sufficiently slender (i.e. relative density below 0.29 [53]), we have neglected the contribution of the axial compression and shear in the overall deformation of the structure [52]. Rotating the top and bottom parts in opposite directions will result in bending of ligaments in form of a full sine wave shape and so axial deformation of the node along its axis. Placing layers of planar anti-tetra-chiral in a proper orientation such that corresponding nodes in adjacent layers have opposite direction of rotation (i.e. with each layer rotated 90 degrees with respect to an adjacent layer), and connecting them using the nodal design introduced above creates a 3D cellular structure. Fig. 1c shows a schematic of such structure with two layers of planar anti-tetra-chiral where a single node is highlighted in black color and Fig. 1d shows a fabricated sample of the structure.

Here, we present a theoretical relationship between the in-plane deformation and the circular element rotation of the planar anti-tetra-chiral structure, and we compare the analytical results with the results obtained using both detailed numerical simulations, as well as the results from a limited number of experiments. Next, the effect of the geometry of node on the amount of rotation associated with the out-of-plane deformation is investigated using analytical and numerical investigations, and verified experimentally. Finally, by eliminating the rotation from the two aforementioned expressions, a relationship between in-plane deformation and out-of-plane deformation for the final 3D structure is derived and the Poisson's ratio is calculated in terms of the geometrical parameters involved in the problem.

To derive an expression relating rotation of the circular element to in-plane deformation in the 2D anti-tetra-chiral structure, we assume an infinite structure and focus our study on the periodic unit cell of this structure, which is shown as an insert in Fig. 1b. The involved geometrical parameters are the circular element diameter D, the length of ligaments a (i.e. center to center distance of circular element) and the thickness of ligaments t, so that  $t \ll a$ . In our calculations we assume that the circular elements retain their original shape as the structure deforms (i.e., they only undergo rigid-body motion and remain as circles) [52,54]. The infinite structure assumption requires zero rotation on the outer vertices of the unit cell (i.e. 8 nodes that are highlighted in blue in

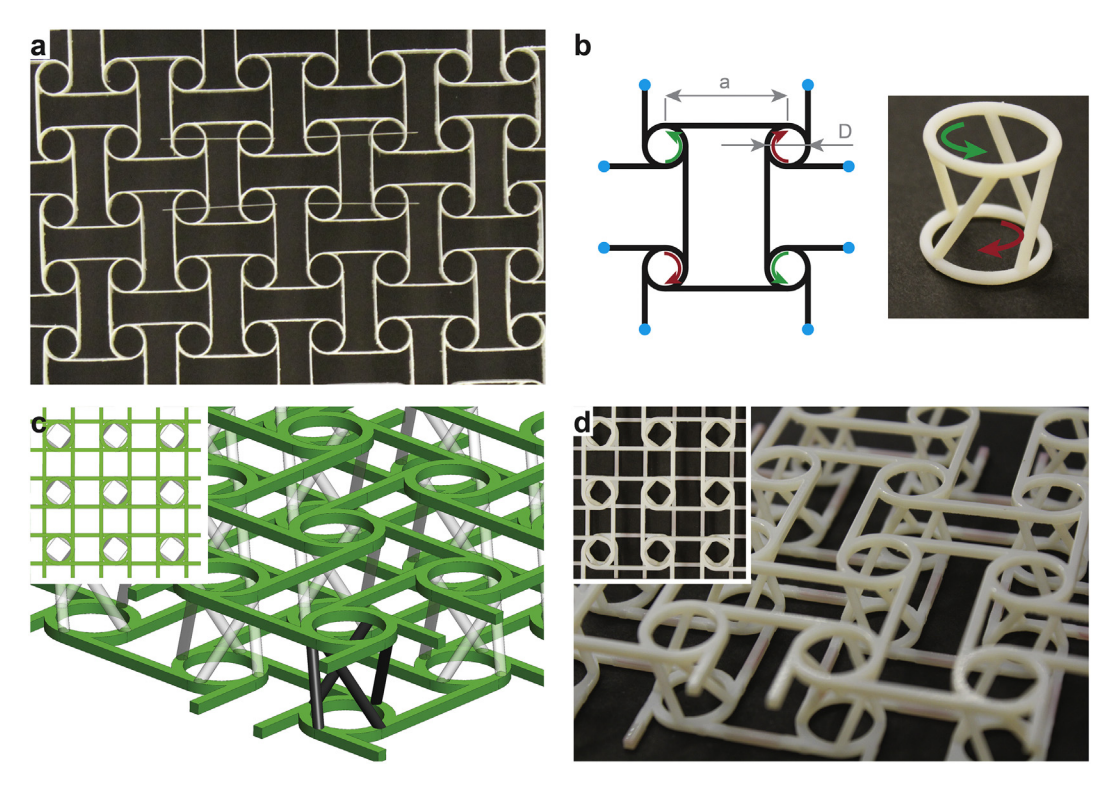


**Fig. 1.** (a) 3D printed anti-tetra-chiral structure that is the base topology for the proposed cellular material in this study. (b) Schematic unit cell of anti-tetra-chiral structure showing rotation direction of nodes and 3D printed sample of the node design used to expand the 2D structure in the out-of-plane direction. (c) Computer aided design model and (d) 3D printed sample of the proposed structure. Inserts show top view.

Fig. 1b). For simplicity, an arc deformed shape is assumed for the ligaments so that one can derive the equation relating the in-plane deformation,  $\varepsilon_{x_0}$  to the node rotation  $\lambda$  as follows:

$$\left(\frac{1}{\lambda} - \frac{D}{a}\right) \sin \lambda = 1 - \varepsilon_{x} \tag{1}$$

where a is the ligament length and D is the circular element diameter (see Supporting information for a detailed derivation). In Fig. 2a, we compared the analytical results with the results obtained from detailed finite element based simulations for D/a = 0.5, as well as experiments. The finite element simulations were carried out using ABAOUS 6.13-2 (SIMULIA, Providence, RI) on the unit cell of the structure in large deformation regime and using in-plane 2 node beam elements for meshing the model (B21 beam elements in ABAQUS). A mesh sensitivity study was carried out to ensure that the results are minimally sensitive to the element size. In these simulations a rectangular cross section of B  $\times$  *t* = 0.4 mm  $\times$  20 mm was assigned to each beam element, which was consistent with our experiments. The material was assumed to be linear elastic with elastic modulus of  $E_s = 20$  GPa and Poisson's ratio of  $\nu = 0.3$ . Numerical simulations were carried out to the point of initial self-contact in the structure. Periodic boundary condition was imposed using geometrical constraints (i.e., coupling interaction between unit cell's edge nodes) to relate the displacements of the corresponding edge nodes, as described in detail in our previous studies [18,55]. For the experiments, the samples were 3D printed out of VeroWhitePlus material on an Eden260V machine (Stratasys Inc., Eden Pierre, MN). Strain in the x-direction ( $\varepsilon_x$ ) was applied using a universal testing machine (Instron 5594) at the rate of 5 mm/min. In order to eliminate the boundary effects, large samples made from total of sixteen unit cells (four by four) were used. The rotation of circular elements was measured in the middle of the sample. Images of the deformed shape of the structure were captured during the course of the compression using a digital camera and the rotation of the circular elements was measured by processing the digital images. It is evident that Eq. (1) can accurately predict the rotation of the node up to a relatively large strain (around  $\varepsilon_x = 0.3$ ). This validation of the derived equation paves the way to construct a map for the rotation of circular element in terms of the applied in-plane strain and D/a ratio. Fig. 2b shows this map for  $0 \le D/a \le 1$  and strain values up to 0.3. This map indicates a wide range of achievable rotations: it also shows that nodes with a low value of D/a can achieve larger rotations. The described mechanism works until the ligaments get in contact with each other, from where the node rotation does not follow the derived equation. We label this region as "self-contact" in Fig. 2b, and the governing equation can be expressed in terms of the geometry of the unit cell (see Supporting information, Eq. S6, for a detailed description).

To this point, by employing a planar anti-tetra-chiral structure, we achieved a circular element rotation that depends on the applied inplane deformation and the normalized parameter, D/a. The next step is to harness this rotation to control out-of-plane deformation. To this end, we propose a design in which oblique ligaments in conjunction with in-plane circular element of the anti-tetra-chiral structure, translate the circular element rotation to out-of-plane deformation and vice versa. There are two parameters that define the behavior of this node design: i) the revolution angle of ligaments  $\gamma$ , which is the angle that each individual oblique ligament's end has revolved with respect to its starting point and, ii) the node diameter to height ratio, D/h. The diameter of cross section of these ligaments, d, would have minimal effect on the deformation mode of the nodes so long as the ligaments are sufficiently slender [52]. For the revolution angle (and also the direction of rotation of the top of the node), we define the counterclockwise rotation as positive, with a feasible range of  $-\pi < \gamma < \pi$ . The top and bottom circular elements of the node always rotate in opposite directions as described before (see Fig. 1b), causing the node height to decrease for co-directional revolution angle and circular element rotation. On the other hand, for a positive revolution angle, a negative node rotation (or vice versa) increases the height until the ligaments become aligned with the node axis (out-of-plane direction). Here, we present a theoretical relationship to describe the out-of-plane deformation in terms of circular element rotation for given D/a and  $\gamma$ . In deriving this analytical expression, the oblique ligaments are considered as fixed-ends beams with a central symmetry, whereby each part is assumed to deform as an arc and the whole ligament is wrapped around a cylinder (see Supporting information and Figs. S3 and S4 for a detailed description). The top and bottom parts of the node are assumed to have no deformation, except for translation in the out-of-plane direction (i.e. z-direction, Fig. 3a insert). These assumptions, which we will show hold true over most of the operation span of the node, yield the following set of nonlinear equations:

$$\frac{L(x \sin\alpha - z \cos\alpha)}{x^2 + z^2} = \sin^{-1}\left(\frac{x \sin\alpha - z \cos\alpha}{\sqrt{x^2 + z^2}}\right)$$
 (2)

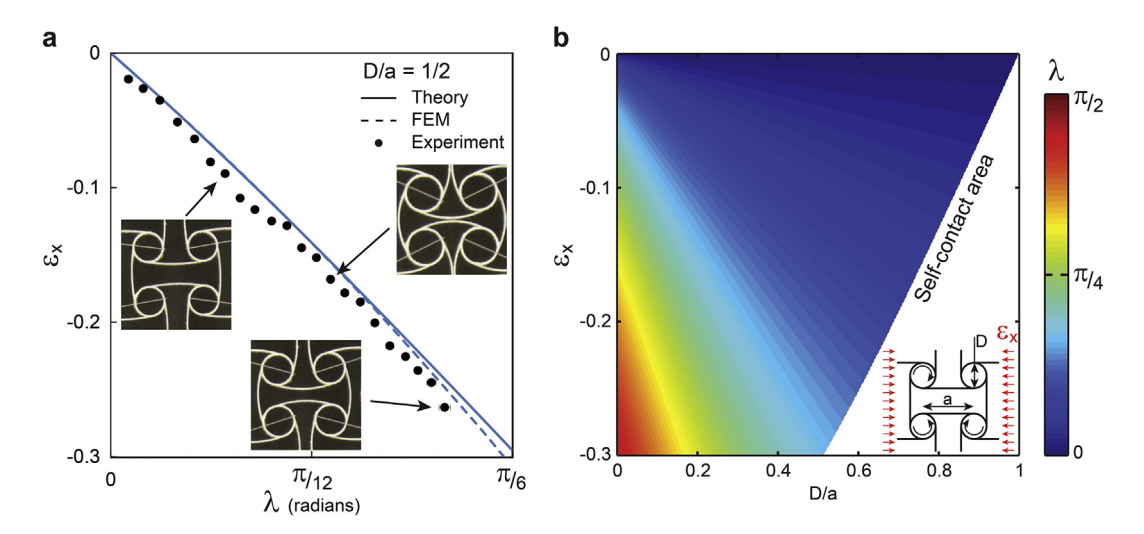


Fig. 2. (a) Nodal rotation versus applied strain  $\varepsilon_x$  for anti-tetra-chiral structure with D/a=1/2, based on analytical predictions, finite element simulation, and experiments. Inserts show deformed configuration of the structure at three different values of strain. (b) Nodal rotation plotted in terms of applied strain and D/a ratio from the analytical prediction.

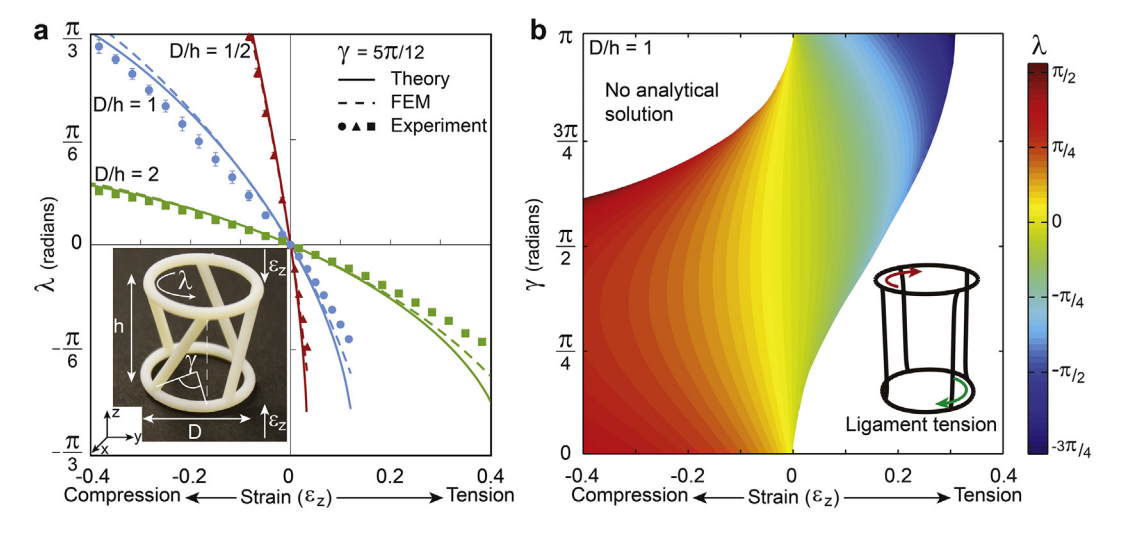


Fig. 3. (a) Nodal rotation versus applied strain  $\varepsilon_z$  for three nodes with D/h=1/2, 1, and 2, based on analytical predictions, FE, and experiments. The revolution angle in all three nodes is  $\gamma=5\pi/12$ . The bars show standard deviation in the experimental results. The responses of nodes with D/h=1/2 and 1 are plotted up to  $\varepsilon_z=0.03$  and 0.12, respectively, where the struts start undergoing tension. (b) Nodal rotation plotted in terms of applied strain and positive values of revolution angle for a node with D/h=1 from the analytical prediction.

$$\frac{2x}{D\cos\left(\frac{\gamma}{2}\right)} = \lambda \left(1 + \frac{\tan\left(\frac{\gamma}{2}\right)}{\tan\left(\frac{\lambda}{2}\right)}\right) \tag{3}$$

where *L* is the initial length of the ligament;  $\alpha = \cos^{-1}(\frac{D \sin \frac{\gamma}{2}}{L})$  is the inclination angle of the ligament with respect to the horizontal plane; and z = $h(1 - \varepsilon_z)$  and x are the projected length of the ligament in the out-ofplane and in-plane directions respectively. By eliminating x from Eqs. (2) and (3), one can calculate the out-of-plane deformation in terms of  $\lambda$  and in-plane deformation. This equation is plotted for three specific cases in Fig. 3a, where the node rotation is shown in terms of strain in the z-direction (i.e. direction of the axis of the cylinder) for three values D/h = 0.5, 1 and 2, with all having a revolution angle  $\gamma = 5\pi/12$ . The figure also includes results from experiments and finite element simulations, which show a very good agreement with the analytical solution. For the experiments, specimens consisting of two layers of the proposed node design (i.e. two nodes connected along the axis of their cylinder) with opposite revolution angle were fabricated from VeroWhitePlus material using 3D printing with the above mentioned values of D, h and  $\gamma$ , where h = 15 mm. All ligaments and circular elements had circular cross section of d = 0.8 mm. The top and bottom circular elements were fixed, and the rotation of the middle circular element was measured using digital imaging at different compressive or tensile strains. Tests were repeated with at least four specimens, and the mean values along with the standard deviation were plotted. Simulations were carried out using ABAQUS and models were meshed by three dimensional 2-node beam elements (i.e. B31 elements). A mesh density study was performed to ensure mesh-size independency and a circular cross section of d=0.8mm was assigned to oblique ligaments, consistent with our experiments. The results in Fig. 3a show that the rate of increase in rotation caused by increasing the out-of-plane strain is highest for the smallest D/h ratio, which suggests that for a specific rotation of the node ends, the out-ofplane deformation for nodes with larger D/h is larger.

Eqs. (2) and (3) can be used to construct a design map for the proposed node spanned by two parameters –revolution angle and out-of-plane deformation, Fig. 3b. The results highlight the behavior of the node for D/h = 1 over a wide range of compressive and tensile strains in the z-direction. This figure indicates the wide range of rotation for the node –as low as  $-\pi/2$  and as high as  $3\pi/4$  – achieved by changing a single geometrical parameter, the revolution angle  $\gamma$ . As mentioned before, there are two limits in the node's performance bracket. The first one stems from the fact that rotation in the node is only possible in

the presence of oblique ligaments. In case of tension, the node will rotate up until the point where all ligaments become aligned with the node axis (out-of-plane direction). Further increasing the tensile strain in the out-of-plane direction will result in stretching ligaments without further nodal rotation. The maximum out-of-plane tensile strain associated with the onset of ligaments tension is easy to calculate since it is basically the difference between the ligaments' length and node initial height. This region is labeled as "ligament tension" in the map. The second limitation corresponds to a region for which a solution to the system of nonlinear Eqs. (2) and (3) cannot be found analytically. Although there might be node rotation in this region as well, the analytical derivation fails to produce a solution.

The proposed node design, with its broad range of achievable node rotation, enables the expansion of the previously discussed 2D antitetra-chiral structures in the third (out of plane) direction to produce 3D cellular structure. We can directly relate in-plane compression (xor y-direction) to out-of-plane deformation (z-direction) by eliminating the node rotation from the deformation equations for the 2D structure and 3D note design. Fig. 4a shows this dependency for a structure with D/h = 1, D/a = 1/2 and two values of  $\gamma = 5\pi/12$  and  $-5\pi/12$ . Eliminating the rotation  $\lambda$ , from Eqs. (1)–(3) yields an analytical prediction relating  $\varepsilon_z$  to  $\varepsilon_x$ , which is shown in Fig. 4a with a solid line. Finite element simulation were carried out on the unit cell of the 3D structure meshed with three dimensional two-node beam elements and the results are reported for comparison. The geometrical parameters of the model were the same as above with h = 15 mm. A circular cross section was assigned to the ligaments with d = 0.8 mm. Experimental results are also provided to verify the simulation and analytical results. Specimens were 3D printed from VeroWhite material with each specimen being constructed of two layers of planar anti-tetra-chiral. Each planar layer has four nodes in both the x and y-directions. A small pin was attached to the bottom circular element of the middle nodes and its displacement with respect to the top circular element was measured using digital imaging at different in-plane compressions. The experimental and finite element simulation results show a very good agreement with the analytical results. The Poisson's ratio in the z-direction,  $v_{xz}$ , can be calculated from the calculated strain, and is plotted in Fig. 4b. Two clearly distinguishable regions with positive Poisson's ratio close to 1 and negative Poisson's ratio close to -1 can be identified for the two structures, which have identical geometry except for the revolution angle. This figure highlights the potential of this design to tune the behavior of 3D cellular structure expansively only by tuning a simple geometrical parameter. We used the analytical expression for the

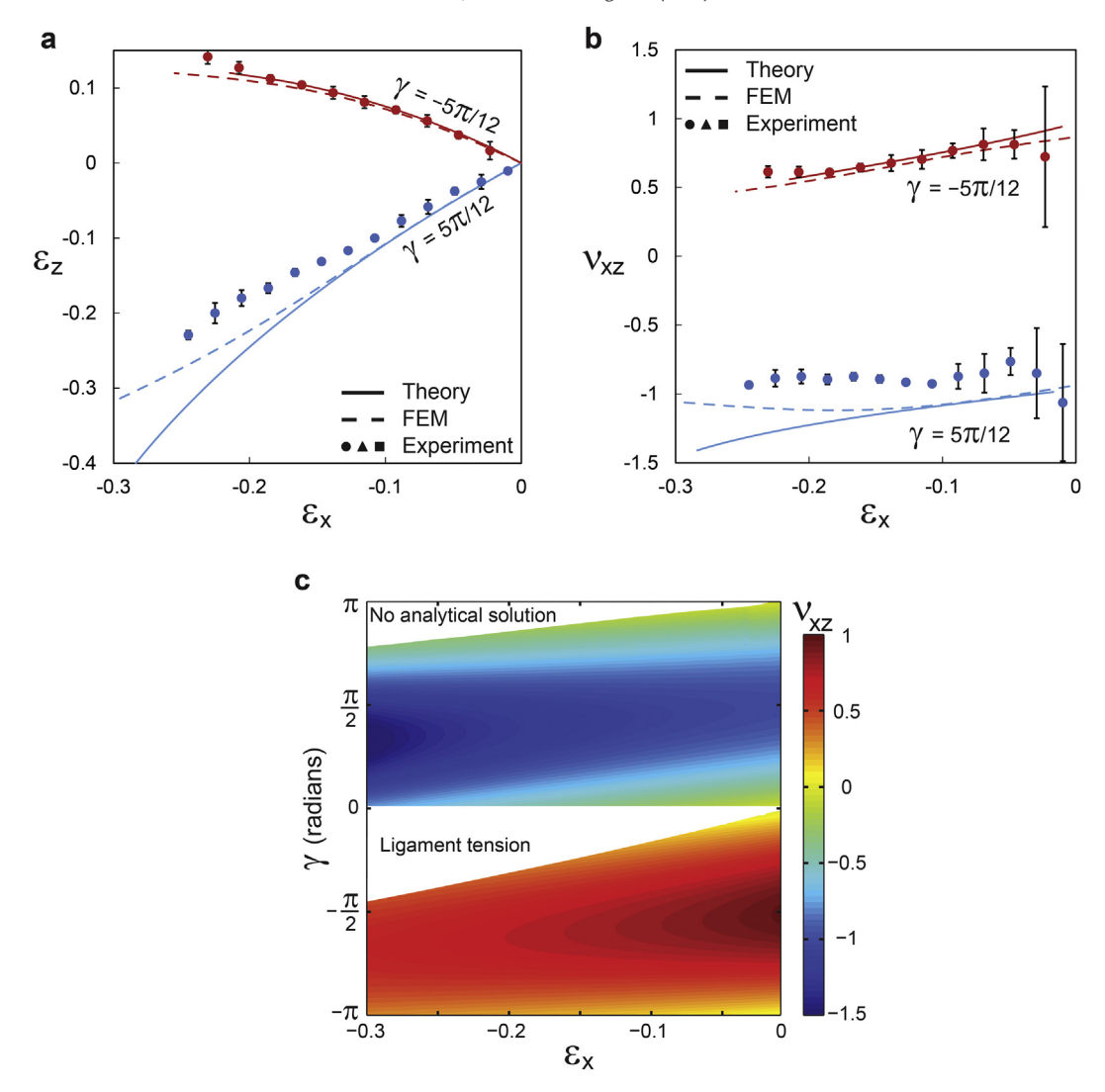


**Fig. 4.** (a) Strain in *z*-direction and (b) Poisson's ratio ( $\nu_{xz}$ ) versus applied strain in *x*-direction for the cases of  $\gamma = 5\pi/12$  and  $\gamma = -5\pi/12$ . Results show good agreement between analytical, finite element, and experimental results. (c) Poisson's ratio ( $\nu_{xz}$ ) map of the 3D anti-tetra-chiral structure in terms of the applied strain ( $\varepsilon_x$ ) and the revolution angle ( $\gamma$ ). In these plots D/h = 1 and D/a = 1/2.

Poisson's ratio to construct a map, Fig. 4c, spanning over the revolution angle and in-plane compression ranges to further emphasize on the applicability of the design over a vast performance regime. This figure shows the Poisson's ratio in the z-direction,  $v_{xz}$ , in terms of the revolution angle  $\gamma$  and the in-plane compression for a 3D structure with D/h = 1, D/a = 1/2. The achievable Poisson's ratios for this specific setting lie between  $-1.5 < v_{xz} < 1$  and the two aforementioned impractical regions are evident. We carried out a limited number of simulations to investigate the elastic response of the proposed 3D cellular metamaterial (see Supporting information for more details). Our results showed that the elastic modulus of the structure can be estimated from the equation proposed by Gibson et al. [53] for open cell foams,  $E/E_s = C\rho^2$ , where C = 0.1368,  $E = C\rho^2$ , where C = 0.1368,  $E = C\rho^2$ , are elastic moduli of the 3D structure and parent material, respectively, and  $\rho$  is the relative density of structure.

In summary, a unique node design consisting of oblique ligaments is introduced, and used to connect layers of anti-chiral planar structures to construct a three-dimensional cellular metamaterial. This relatively simple design enables us to achieve a wide range of Poisson's ratios of the resultant 3D cellular metamaterial by adjusting only three geometrical parameters. Using ligaments with different revolution angles in a single node provides the proposed unique node design with additional degrees of freedom corresponding to bending with respect to the *x*- or

y-directions, which can lead to potential application in developing novel actuators [56]. The node design concept proposed here can be applied to other types of planar structure, such as rotating-units structures [16,27] and structures with isotropic negative Poisson's ratio [24], thus providing a framework for developing three dimensional lattices and cellular metamaterials with strong auxetic behavior.

### Acknowledgement

This work was supported by the United States National Science Foundation's Civil, Mechanical, and Manufacturing Innovation Grant No. 1634560.

## Appendix A. Supplementary data

Supplementary data to this article can be found online at https://doi.org/10.1016/j.matdes.2018.02.052.

#### References

 S. Lubkin, Unidirectional waves on rings: models for chiral preference of circumnutating plants, Bull. Math. Biol. 56 (1994) 795–810.

- [2] M. Oliverio, M.C. Digilio, P. Versacci, B. Dallapiccola, B. Marino, Shells and heart: are human laterality and chirality of snails controlled by the same maternal genes? Am. J. Med. Genet. A 152A (2010) 2419–2425.
- [3] M. Schilthuizen, A. Davison, The convoluted evolution of snail chirality, Naturwissenschaften 92 (2005) 504–515.
- [4] Z.-L. Zhao, B. Li, X.-Q. Feng, Handedness-dependent hyperelasticity of biological soft fibers with multilayered helical structures, Int. J. Non Linear Mech. 81 (2016) 19–29.
- [5] R.R. Sinden, DNA Structure and Function, Academic Press, San Diego, 1994.
- [6] Z. Li, R. Zhao, T. Koschny, M. Kafesaki, K.B. Alici, E. Colak, H. Caglayan, E. Ozbay, C.M. Soukoulis, Chiral metamaterials with negative refractive index based on four "U" split ring resonators, Appl. Phys. Lett. 97 (2010), 081901.
- [7] E. Plum, J. Zhou, J. Dong, V.A. Fedotov, T. Koschny, C.M. Soukoulis, N.I. Zheludev, Metamaterial with negative index due to chirality, Phys. Rev. B 79 (2009), 035407.
- [8] S. Zhang, Y.-S. Park, J. Li, X. Lu, W. Zhang, X. Zhang, Negative refractive index in chiral metamaterials, Phys. Rev. Lett. 102 (2009), 023901
- [9] J. Zhou, J. Dong, B. Wang, T. Koschny, M. Kafesaki, C.M. Soukoulis, Negative refractive index due to chirality, Phys. Rev. B 79 (2009), 121104.
- [10] A. Spadoni, M. Ruzzene, Static aeroelastic response of chiral-core airfoils, J. Intell. Mater. Syst. Struct. 18 (2007) 1067–1075.
- [11] D. Bornengo, F. Scarpa, C. Remillat, Evaluation of hexagonal chiral structure for morphing airfoil concept, Proc. Inst. Mech. Eng. G J. Aerosp. Eng. 219 (2005) 185–192
- [12] H.M.A. Kolken, A.A. Zadpoor, Auxetic mechanical metamaterials, RSC Adv. 7 (2017) 5111–5129.
- [13] D. Mousanezhad, B. Haghpanah, R. Ghosh, A.M. Hamouda, H. Nayeb-Hashemi, A. Vaziri, Elastic properties of chiral, anti-chiral, and hierarchical honeycombs: a simple energy-based approach, Theor. Appl. Mech. Lett. 6 (2016) 81–96.
- [14] D. Mousanezhad, S. Babaee, H. Ebrahimi, R. Ghosh, A.S. Hamouda, K. Bertoldi, A. Vaziri, Hierarchical honeycomb auxetic metamaterials, 5 (2015), 18306.
- [15] A. Rafsanjani, D. Pasini, Bistable auxetic mechanical metamaterials inspired by ancient geometric motifs, Extreme Mech. Lett. 9 (Part 2) (2016) 291–296.
- [16] J.N. Grima, K.E. Evans, Auxetic behavior from rotating squares, J. Mater. Sci. Lett. 19 (2000) 3.
- [17] S. Babaee, J. Shim, J.C. Weaver, E.R. Chen, N. Patel, K. Bertoldi, 3D soft metamaterials with negative Poisson's ratio. Adv. Mater. 25 (2013) 5044–5049.
- [18] D. Mousanezhad, H. Ebrahimi, B. Haghpanah, R. Ghosh, A. Ajdari, A.M.S. Hamouda, A. Vaziri, Spiderweb honeycombs, Int. J. Solids Struct. 66 (2015) 218–227.
- [19] J. Shim, C. Perdigou, E.R. Chen, K. Bertoldi, P.M. Reis, Buckling-induced encapsulation of structured elastic shells under pressure, Proc. Natl. Acad. Sci. 109 (2012) 5978–5983
- [20] K. Bertoldi, P.M. Reis, S. Willshaw, T. Mullin, Negative Poisson's ratio behavior induced by an elastic instability, Adv. Mater. 22 (2010) 361–366.
- [21] J. Shim, S. Shan, A. Kosmrlj, S.H. Kang, E.R. Chen, J.C. Weaver, K. Bertoldi, Harnessing instabilities for design of soft reconfigurable auxetic/chiral materials, Soft Matter 9 (2013) 8198–8202.
- [22] B. Haghpanah, L. Salari-Sharif, P. Pourrajab, J. Hopkins, L. Valdevit, Multistable shape-reconfigurable architected materials, Adv. Mater. 28 (2016) 7915–7920.
- [23] T.A.M. Hewage, K.L. Alderson, A. Alderson, F. Scarpa, Double-negative mechanical metamaterials displaying simultaneous negative stiffness and negative Poisson's ratio properties, Adv. Mater. 28 (2016) 10323–10332.
- [24] S. Shan, S.H. Kang, Z. Zhao, L. Fang, K. Bertoldi, Design of planar isotropic negative Poisson's ratio structures, Extreme Mech. Lett. 4 (2015) 96–102.
- [25] R. Lakes, Foam structures with a negative poisson's ratio, Science 235 (1987).
- [26] K.E. Evans, M.A. Nkansah, I.J. Hutchinson, S.C. Rogers, Molecular network design, Nature 353 (1991) 124.
- [27] J.N. Grima, K.E. Evans, Auxetic behavior from rotating triangles, J. Mater. Sci. 41 (2006) 4.
- [28] Y. Cho, J.-H. Shin, A. Costa, T.A. Kim, V. Kunin, J. Li, S.Y. Lee, S. Yang, H.N. Han, I.-S. Choi, D.J. Srolovitz, Engineering the shape and structure of materials by fractal cut, Proc. Natl. Acad. Sci. U. S. A. 111 (2014) 17390–17395.
- [29] W. Marius, C. Tian, S. Kristina, Large shape transforming 4D auxetic structures, 3D Printing and Additive Manufacturing, 2017 September 2017, ahead of print.
- [30] H. Ebrahimi, D. Mousanezhad, B. Haghpanah, R. Ghosh, A. Vaziri, Lattice materials with reversible foldability, Adv. Eng. Mater. 19 (2017) (1600646-n/a).

- [31] J.B. Choi, R.S. Lakes, Design of a fastener based on negative Poisson's ratio foam, Cell. Polym. 10 (1991) 8.
- [32] F. Scarpa, Auxetic materials for bioprostheses [in the spotlight], IEEE Signal Process. Mag. 25 (2008) (128-126).
- [33] R. Gatt, R. Caruana-Gauci, D. Attard, A.R. Casha, W. Wolak, K. Dudek, L. Mizzi, J.N. Grima, On the properties of real finite-sized planar and tubular stent-like auxetic structures, Phys. Status Solidi B 251 (2014) 321–327.
- [34] L. Mizzi, D. Attard, A. Casha, J.N. Grima, R. Gatt, On the suitability of hexagonal honeycombs as stent geometries, Phys. Status Solidi B 251 (2014) 328–337.
- [35] T.W. Tan, G.R. Douglas, T. Bond, A.S. Phani, Compliance and longitudinal strain of cardiovascular stents: influence of cell geometry, J. Med. Devices 5 (2011) (041002-041002-041006).
- [36] F. Scarpa, F. Smith, B. Chambers, G. Burriesci, Mechanical and electromagnetic behaviour of auxetic honeycomb structures, Aeronaut. J. 107 (2003) 175–183.
- [37] K.E. Evans, K.L. Alderson, Auxetic materials: the positive side of being negative, Eng. Sci. Educ. J. 9 (2000) 148–154.
- [38] J. Bauer, L.R. Meza, T.A. Schaedler, R. Schwaiger, X. Zheng, L. Valdevit, Nanolattices: an emerging class of mechanical metamaterials, Adv. Mater. 29 (2017) (1701850-n/a).
- [39] F. Scarpa, L.G. Ciffo, J.R. Yates, Dynamic properties of high structural integrity auxetic open cell foam, Smart Mater. Struct. 13 (2004) 49.
- [40] X.-T. Wang, B. Wang, X.-W. Li, L. Ma, Mechanical properties of 3D re-entrant auxetic cellular structures, Int. J. Mech. Sci. 131-132 (2017) 396–407.
- [41] L. Yang, O. Harrysson, H. West, D. Cormier, Mechanical properties of 3D re-entrant honeycomb auxetic structures realized via additive manufacturing, Int. J. Solids Struct. 69-70 (2015) 475–490.
- [42] M. Shokri Rad, Y. Prawoto, Z. Ahmad, Analytical solution and finite element approach to the 3D re-entrant structures of auxetic materials, Mech. Mater. 74 (2014) 76–87.
- [43] W. Franziska, O. Fuad, A. Lucas, A.L. Matthias, K. Carolin, Fabrication and characterisation of a fully auxetic 3D lattice structure via selective electron beam melting, Smart Mater. Struct. 26 (2017), 025013.
- [44] L. Yang, O. Harrysson, H. West, D. Cormier, Compressive properties of Ti–6Al–4V auxetic mesh structures made by electron beam melting, Acta Mater. 60 (2012) 3370–3379
- [45] X. Li, Z. Lu, Z. Yang, C. Yang, Directions dependence of the elastic properties of a 3D augmented re-entrant cellular structure. Mater. Des. 134 (2017) 151–162.
- [46] R. Xin, S. Jianhu, G. Arash, T. Hongqi, X. Yi Min, Experiments and parametric studies on 3D metallic auxetic metamaterials with tuneable mechanical properties, Smart Mater. Struct. 24 (2015), 095016.
- [47] J. Shen, S. Zhou, X. Huang, Y.M. Xie, Simple cubic three-dimensional auxetic metamaterials, Phys. Status Solidi B 251 (2014) 1515–1522.
- [48] Z. Lu, Q. Wang, X. Li, Z. Yang, Elastic properties of two novel auxetic 3D cellular structures, Int. J. Solids Struct. 124 (2017) 46–56.
- [49] H. Chan Soo, E.P. Michael, S.L. Roderic, Chiral three-dimensional lattices with tunable Poisson's ratio, Smart Mater. Struct. 25 (2016), 054005.
- [50] T. Bückmann, N. Stenger, M. Kadic, J. Kaschke, A. Frölich, T. Kennerknecht, C. Eberl, M. Thiel, M. Wegener, Tailored 3D mechanical metamaterials made by dip-in direct-laser-writing optical lithography, Adv. Mater. 24 (2012) 2710–2714.
- [51] B. Tiemo, S. Robert, T. Michael, K. Muamer, W.M. Graeme, W. Martin, On three-dimensional dilational elastic metamaterials, New J. Phys. 16 (2014), 033032.
- [52] D. Prall, R.S. Lakes, Properties of a chiral honeycomb with a Poisson's ratio of 1, Int. J. Mech. Sci. 39 (1997) 305–314.
- [53] L.J. Gibson, M.F. Ashby, Cellular Solids: Structure and Properties, Cambridge University Press, 1999.
- [54] A. Alderson, K.L. Alderson, D. Attard, K.E. Evans, R. Gatt, J.N. Grima, W. Miller, N. Ravirala, C.W. Smith, K. Zied, Elastic constants of 3-, 4- and 6-connected chiral and anti-chiral honeycombs subject to uniaxial in-plane loading, Compos. Sci. Technol. 70 (2010) 1042–1048.
- [55] A. Ajdari, H. Nayeb-Hashemi, A. Vaziri, Dynamic crushing and energy absorption of regular, irregular and functionally graded cellular structures, Int. J. Solids Struct. 48 (2011) 506–516.
- [56] A. Lazarus, P.M. Reis, Soft actuation of structured cylinders through auxetic behavior, Adv. Eng. Mater. 17 (2015) 815–820.